Supporting information for

6-Aza-2-thio-thymine-gold Nanocluster: An Excellent Candidate in Gold Nanocluster-based Photoelectrochemical Field

Yu Yang,‡[a] Chaoguo Wei,‡[a] Wenjun Wang,[a] Hamada A. A. Noreldeen,[a] Zhongnan Huang,[a] Haohua Deng,[a] Huaping Peng,[a,*] Xinghua Xia,[b] and Wei Chen[a,*]

[a] Higher Educational Key Laboratory for Nano Biomedical Technology of Fujian Province, Department of Pharmaceutical Analysis, Faculty of Pharmacy, Fujian Medical University, Fuzhou 350004, China

[b] State Key Laboratory of Analytical Chemistry for Life Science and Collaborative Innovation Center of Chemistry for Life Sciences, School of Chemistry and Chemical Engineering, Nanjing University, Nanjing 210093, China

E-mail: chenandhu@163.com (Wei Chen); phpfjmu@126.com, penghuaping@fjmu.edu.cn (H.P. Peng)

Experimental Section

Chemicals and Materials: All chemicals and solvents were at least of analytical grade and used as received. Aqueous solutions in all experiments were prepared using deionized water. 6-Aza-2-thiothymine (ATT), glutathione (GSH), and bovine serum albumin (BSA) were purchased from Alfa Aesar Chemicals Co.Ltd. Chloroauric acid ($HAuCl_4 \cdot 3H_2O$), sodium borohydride ($NaBH_4$) and NaOH were bought from Aladdin Reagent Co. (Shanghai, China). Na_2HPO_4, NaH_2PO_4, NaOH, ethanol, and HNO_3 were purchased from Sinopharm Chemical Reagent Company (China). Phosphate buffer solution (PB, 0.1 M, pH 2) was used in photoelectrochemistry and photoelectrochemical experiments. Tetrabutylammonium hexafluorophosphate were purchased from Sigma-Aldrich. All glassware was cleaned with aqua regia and rinsed with water prior to use.

Apparatus and Characterization: All ultraviolet-visible (UV-vis) absorption spectra were recorded using a UV-2450 UV-vis spectrophotometer (Shimadzu). The PL spectra were performed on a Cary Eclipse fluorescence spectrophotometer (Agilent). Transmission electron microscopy (TEM) images were taken on a JEM-2100 microscope (JEOL). The UPS were performed on a Escalab 250xi (Thermo Fisher Scientific). The electrochemical impedance spectroscopy (EIS) was performed at a Autolabe (Metrohm). The relative permittivity was performed on a Vector Network Analyzer PNA-N5244A (Agilent). Electron paramagnetic resonance (EPR) experiments were conducted on a Bruker A300 spectrometer (Bruker Co., Germany).

Synthesis of ATT-AuNCs: ATT-AuNCs were synthesized according to the method reported in our previous study[1]. ATT (4 mL, 80 mM) containing 0.2 M NaOH was added to $HAuCl_4$ solution (4 mL, 10 mg/mL), and the mixed solution was continuously stirred in the dark at room temperature for 1 h. The as-synthesized ATT-AuNCs were purified by ultrafiltration (Millipore, 3.5 kDa). The resulting ATT-AuNCs were stored at 4 °C in the dark prior to use.

Synthesis of GSH-AuNCs: GSH-AuNCs were synthesized according to the previous reported[2]. An aqueous solution of $HAuCl_4$ (200 mM, 1 mL) was mixed with a solution (9 mL) containing GSH (100 mM, 0.4 mL) and ultrapure water (8.6 mL) under gentle stirring. After 30 min incubation at ambient temperature, a portion of the formed Au(I)-GSH complexes (7 mL) was added to an aqueous solution of GSH (100 mM, 2 mL). Subsequently, the mixed solutions were heated up to 70 °C for 24 h, generating the GSH-AuNCs.

Synthesis of BSA-AuNCs: BSA-AuNCs were synthesized according to the previous strategy by Xie and co-authors[3]. All glassware was rinsed thoroughly with freshly prepared Aqua Regia (HCl: HNO_3; 3:1 v/v) and washed with ultrapure bidistilled water. In a typical experiment, 10.0 mM aqueous solution of $HAuCl_4$ (5.0 mL, 37 °C) was added to 5.0 mL of BSA aqueous solution (50.0 mg/mL, 37 °C) under vigorous stirring at 37 °C. After about two minutes, NaOH solution (0.5 mL, 1 mM) was added and the reaction mixture was incubated at 37 °C for 12 h. The color of the reaction mixture changed from light yellow to light brown and then became deep brown as the reaction proceeded. The final synthesized solution of BSA-AuNCs was kept at 4 °C prior to use.

Fabrication of PEC detection system: A bare GCE was polished sequentially with alumina powder (1.0, 0.3, and 0.05 μm) and then sonicated sequentially in HNO_3, ethanol, and water for 3 min each. The cleaned electrode was thoroughly rinsed with water and dried with N_2 immediately. Then, 5 μL of the ATT-AuNCs (2 mg/mL), BSA-AuNCs (2 mg/mL), GSH-AuNCs (2 mg/mL) and ATT (40 mM) solution was dropped on the GCE surface. Subsequent drying in air at room temperature to give the ATT-AuNCs-modified GCE (ATT-AuNCs/GCE), BSA-AuNCs-modified GCE (BSA-AuNCs/GCE), GSH-AuNCs-modified GCE (GSH-AuNCs/GCE) and ATT-modified GCE (ATT/GCE). ATT-AuNCs/GCE, BSA-AuNCs/GCE, GSH-AuNCs/GCE, ATT/GCE and CR-AuNCs/GCE electrode stored at room temperature for further PEC detection.

PEC measurement: All PEC messurements were performed at a CHI 660C electrochemical workstation (Shanghai, CH Instruments, China) accommodated with a three-electrode system. The

modified GCE acted as a working electrode, a platinum wire as a counter electrode and a Ag/AgCl as a reference electrode. Multifunctional LED lamp (PEC-10W, Tianjin Deshang Technology Co. Ltd, China) was used as an irradiation source with the wavelength from 365-840 nm. The incident photon-to-current conversion efficiency (IPCE) was measured as a function of the incident light wavelength (365-840 nm). The illumination intensity at the 365-370 nm was 10 mW/cm^2. The electrolyte was composed of an aqueous solution of 0.1 M phosphate buffer solution (PB, pH 2). The photocurrent of the modified GCE electrode was recorded versus time with alternate light-on and light-off cycles at a fixed bias voltage of 0 V, and the distance was 5 cm between the electrode and the light source. Mott-Schottky plots for the samples were obtained at a frequency of 1.0 KHz, and the electrochemical impedance spectroscopy (EIS) was conducted at a frequency from 0.05 Hz to 100 KHz (*vs.* Ag/AgCl). Differential pulse voltammetry (DPV) of ATT-AuNCs was measured at 0.01 V/s in degassed acetonitrile containing 0.1 M Tetrabutylammonium hexafluorophosphate with ATT-AuNCs/GCE working, platinum wire as reference electrode and counter electrode respectively.

Calculation of applied bias photon-to-current efficiency (ABPE), incident photon-to-current conversion efficiency (IPCE), Mott–Schottky, debye length (L_D) and depletion layer width (W)

Calculation of ABPE: Assuming 100% Faradaic efficiency, the ABPE (Fig. S3A) can be calculated using Equation (S1):

$$\text{ABPE (\%)} = J\,(1.23-V)/P\times 100 \quad \text{(S1)}$$

where J, V, and P are the photocurrent density (mA cm^{-2}), the applied bias (V *vs.* RHE), and the incident light power density (10 mW cm^{-2}), respectively.

Calculation of IPCE: The IPCE was measured as a function of the incident light wavelength (Fig. 1D), and calculated using the following Equation (S2):

$$\text{IPCE (\%)} = 1240\times J/(\lambda\times P_{\text{light}})\times 100 \quad \text{(S2)}$$

where $J(\lambda)$ is the measured photocurrent density at a specific wavelength, λ is the wavelength of the incident light, and $P(\lambda)$ is the measured light power density at that wavelength.

Calculation of Mott–Schottky: The concentration of the materials could be calculated using the Mott–Schottky Eq. (3):[4]

$$1/C^2 = (2/e\varepsilon_0\varepsilon N))[(U - U_{FB}) - kT/e] \quad \text{(S3)}$$

where C is the space charge capacitance, N_A is the acceptor concentration (electron concentration for the p-type semiconductor), e is the electron charge, ε_0 is the permittivity of the vacuum, ε is the relative permittivity (for ATT-AuNCs, GSH-AuNCs, and BSA-AuNCs, ε = 3.15, 2.99, and 3.15 respectively), U is the applied potential, T is the absolute temperature, and k is the Boltzmann constant. At room temperature, the term kT/e was calculated to be 25.7 meV, which is exceedingly small and can be neglected.[5]

The slope determined from the analysis of the Mott–Schottky plot can be used to calculate the concentration using the following equation (S4):[6]

$$N=(2/e\varepsilon_0\varepsilon)[d(1/C^2)/dV]^{-1} \quad \text{(S4)}$$

Calculation of L_D: The Debye length (L_D) was calculated using the following equation (S5):[7]

$$L_D = (\varepsilon_0\varepsilon kT/e^2N_A)^{1/2} \quad \text{(S5)}$$

Calculation of W: The depletion layer width (W) at 0.0 V bias (*vs*. Ag/AgCl) can be calculated using the following equation (S6):[8]

$$W = (2\varepsilon_0\varepsilon (E - E_{FB} - kT/e))/eN_A)^{1/2} \quad \text{(S6)}$$

Characterization of ATT-AuNCs: The morphology and structure of ATT-AuNCs were investigated by transmission electron microscopy (TEM). The TEM image (Fig. S1A) showed that the prepared ATT-AuNCs were nearly spherical in shape and the diameters were average about 2.5 nm (Fig. S1B). As shown in Fig. S1C, the absorption spectrum of ATT-AuNCs exhibited two sharp peaks at 406 nm and 473 nm. These excitonic peaks demonstrated the presence of discrete energy levels.[9] The absorption band at 473 nm probably arised primarily from HOMO→LUMO+2 and HOMO-1→LUMO+2 transitions. In addition, the higher-energy absorption band around 406 nm was probably primarily assigned to HOMO-2→LUMO+2.[10] The 523-nm absorption edge indicated the energy gap of 2.4 eV between the highest occupied molecular orbital (HOMO) and

the lowest unoccupied molecular orbital (LUMO), indicating the semiconducting character that is commonly observed for ligand-protected Au clusters.[11] The fluorescence emission spectrum of the ATT-AuNCs showed an emission maximum at 525 nm (Fig. S1D), the excitation wavelength is 406 and 473 nm, which match well the maxima in the absorption spectra. The absorption and photoluminescence results obtained for GSH-AuNCs (λ_{em} = 611 nm) and BSA-AuNCs (λ_{em} = 650 nm) are shown in Figs. S2. These results corresponded to previous results[1] and indicated the successful synthesis of the AuNCs.

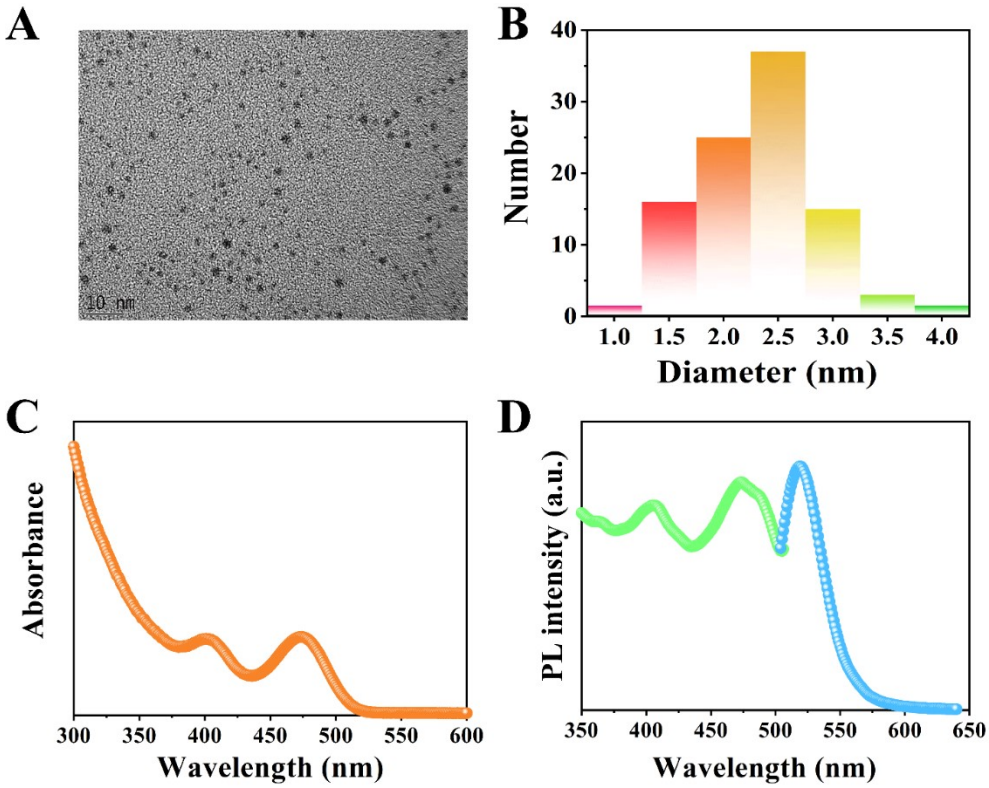

Fig. S1 (A) TEM image of ATT-AuNCs. (B) Particle size distribution image of ATT-AuNCs, (C) UV-vis absorption spectrum of ATT-AuNCs. (D) PL excitation and emission spectra of ATT-AuNCs.

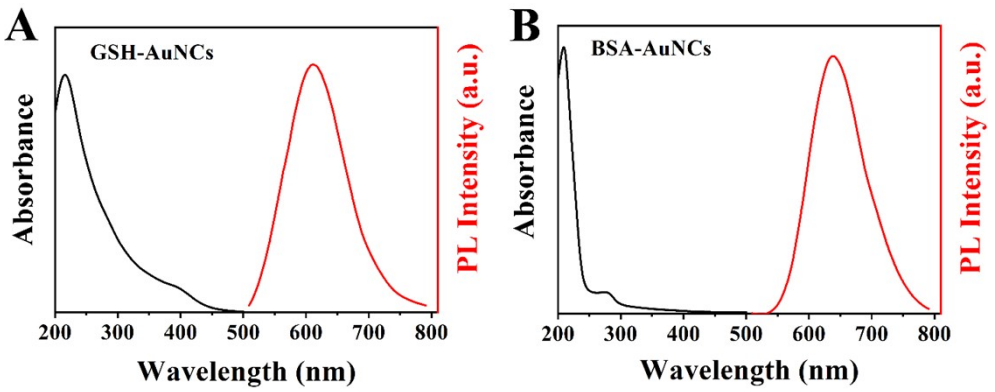

Fig. S2 Absorption and emission spectra of GSH-AuNCs (A) amd BSA-AuNCs (B) in water.

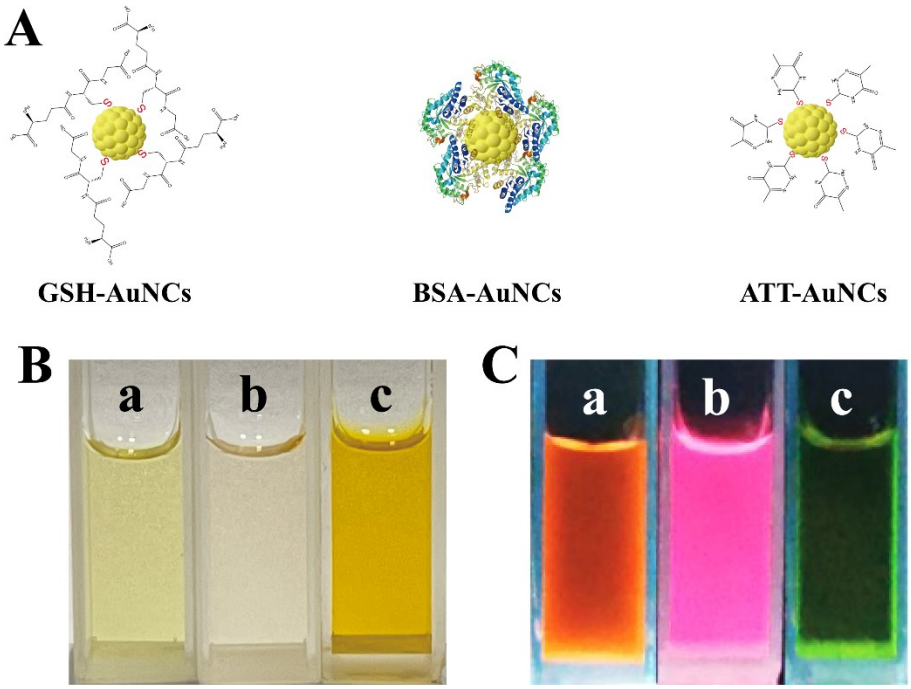

Fig. S3 Gold core and different shells of GSH/BSA/ATT of AuNCs with a chemical structure of the GSH/BSA/ATT (A); Digital images of Au NCs with GSH (a)/BSA (b)/ATT (c) under daylight (B) and UV lamp (C) irradiation.

The FTIR spectrum of the as-prepared ATT-AuNCs, GSH-AuNCs and BSA-AuNCs were further characterized (Fig. S4). It can be seen that the absorption peaks of ATT at 804 cm^{-1} and 3148 cm^{-1} correspond to the stretching vibration of the N-H bond (Fig. S4A).[12] The peaks at 1606 and 1680 cm^{-1} were ascribed to the vibrations of C=O and N=C ring groups, and the broad peak at 3415 cm^{-1} represented the stretching vibration of the hydroxy group. Notably, the absorption peak at 2461 cm^{-1} indicated the characteristic stretching band of the sulfhydryl group, but it disappeared after the formation of ATT-AuNCs. It demonstrates that Au-S bonds were formed between the ligand of ATT and Au core, which also confirm the successfully synthesized of ATT-AuNCs.[13]

As shown in Fig. S4B, the FTIR spectrum of GSH (black curve) revealed characteristic absorption peaks at 2527 (S−H stretching bands), 3125 and 3207 (N−H stretching bands), 1600 and 1713 (C=O stretching bands), and 1538 cm^{-1} (N−H deformation of amide bonds).[14] After the formation of GSH-AuNCs, the FTIR spectrum of glutathione on the GSH-AuNCs exhibited a slight shift and relative broadening compared to that of pure GSH due to a change in the dipole moment of glutathione.[15] Most importantly, S−H stretching bands of GSH disappeared from the FTIR spectrum of GSH-AuNCs. The disappearance of the S−H stretching bands of GSH-AuNCs can be attributed to the formation of Au−S covalent bonds between GSH and AuNCs.[16]

As shown in Fig. S4C, the absorption peaks of pure BSA at 3420, 3055, 1650, and 1539 cm^{-1} were assigned to the stretching vibration of-OH, amide A (mainly-NH stretching vibration), amide I (mainly C=O stretching vibrations), and amide II (the coupling of bending vibrate of N-H and stretching vibrate of C-N) bands, respectively.[17] The difference between the FTIR spectrum of pure BSA and BSA-AuNCs revealed that the characteristic peak of -NH groups disappeared, suggesting that there might be a coordination interaction between Au and -NH groups of BSA. This may play an important role in the formation of AuNCs.

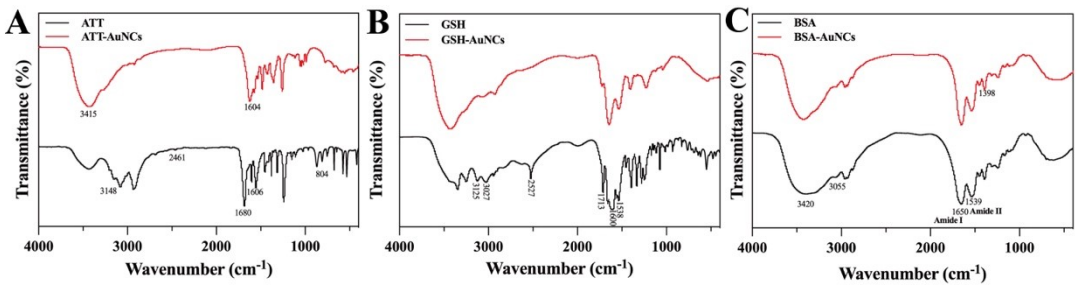

Fig. S4 FTIR spectra characterization of (A) ATT-AuNCs, (B) GSH-AuNCs and (C) BSA-AuNCs and the ligands of the corresponded AuNCs.

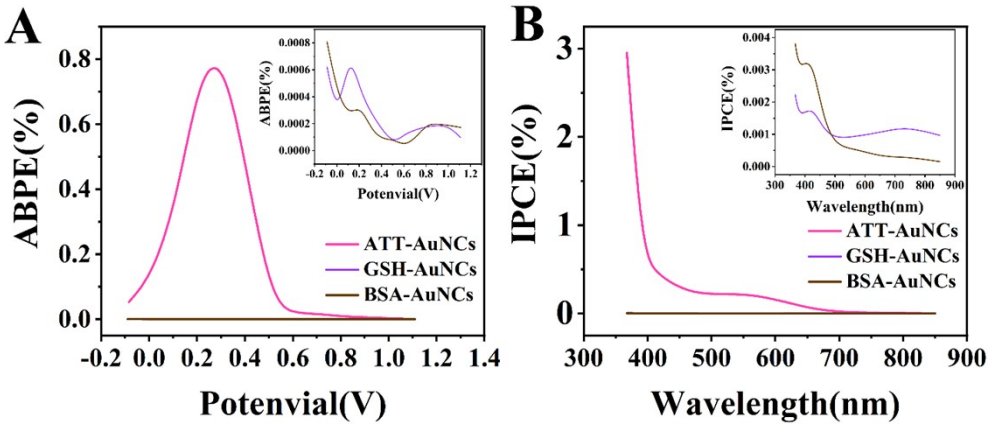

Fig. S5 PEC performances of bare GCE, GSH-AuNCs, BSA-AuNCs and ATT-AuNCs photoelectrodes. (A) ABPE, (B) IPCE at 0 V *vs*. Ag/AgCl for ATT-AuNCs, -0.5 V *vs*. Ag/AgCl for GSH-AuNCs and 0.5 V *vs*. Ag/AgCl for BSA-AuNCs.

TEM images of the ATT-AuNCs modified on GCE surface showed that the morphology of ATT-AuNCs after modified on GCE surface remained spherical in shape, and it existed self-aggregation effect of AuNCs on the electrode surface (Fig. S6). Notably, there was a negligible effect on the morphology and particle size of ATT-AuNCs modified on GCE surface after PEC stability test, which further demonstrated the PEC stability of this ATT-AuNC-based PEC system.

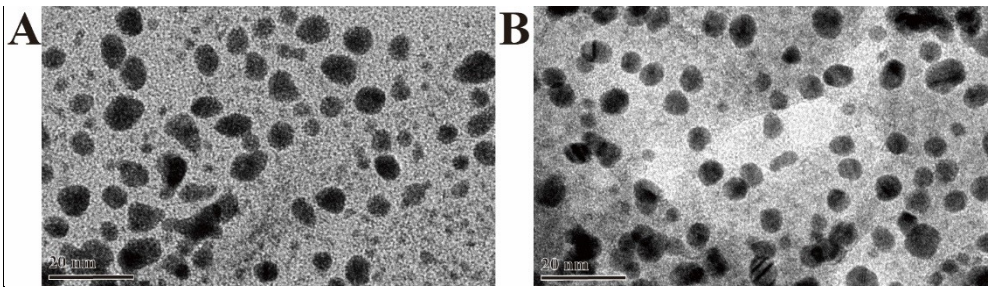

Fig. S6 TEM images of the ATT-AuNCs modified on GCE surface before (A) and after (B) the PEC stability test.

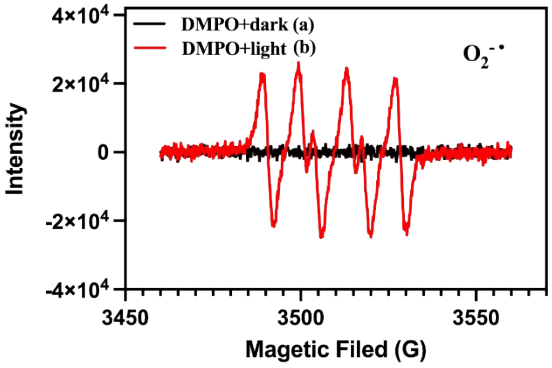

Fig. S7 EPR spectra of the DMPO adduct with $O_2^{-\bullet}$ generated in ATT-AuNC based electrode system under dark (a) and illumination (b) condition in PB solution (pH=2).

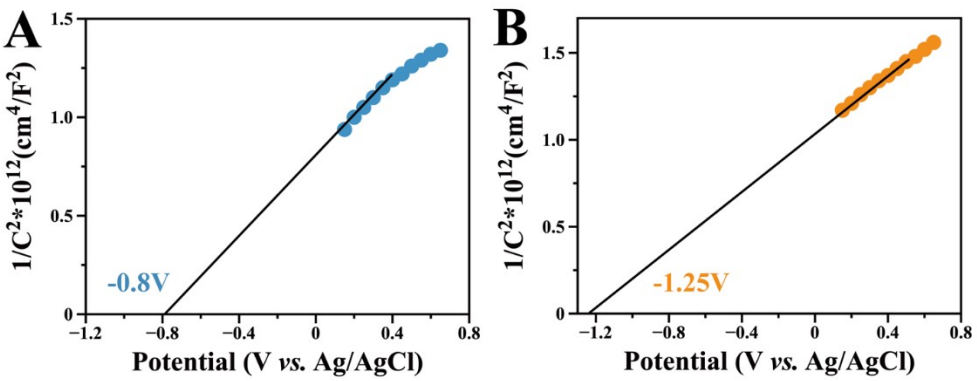

Fig. S8 Mott-Schottky plots of GSH-AuNCs (A) and BSA-AuNCs (B) were measured in an aqueous solution of PB (pH=7.4).

References

1. H. H. Deng, X. Q. Shi, F. F. Wang, H. P. Peng, A. L. Liu, X. H. Xia and W. Chen, *Chem. Mater., 2017*, **29**, 1362–1369.

2. C. C. Huang, Z. Yang, K. H. Lee and H. T. Chang, *Angew. Chem. Int. Ed.*, 2007, **119**, 6948–6952.

3. B. Adhikari and A. Banerjee, *Chem. Mater.*, 2010, **22**, 4364–4371.

4. Yang, X.; Wolcott, A.; Wang, G.; Sobo, A.; Fitzmorris, R. C.; Qian, F.; Zhang, J. Z.; Li, Y, *Nano Lett.*, 2009, **9**, 2331–2336.

5. L. Yu, G. Li, X. Zhang, X. Ba, G. Shi, Y. Li, P. K. Wong, J. C. Yu and Y. Yu, *ACS Catal.*, 2016, **6**, 6444–6454.

6. Z. Zhang and P. Wang, *Energy Environ. Sci.*, 2012, **5**, 6506–6512.

7. X. Wang, J. Xie and C. M. Li, *J. Mater. Chem. A.*, 2015, **3**, 1235–1242.

8. J. M. Gurrentz and M. J. Rose, *J. Am. Chem. Soc.*, 2020, **142**, 5657–5667.

9. F. Hu, Z.-J. Guan, G. Yang, J.-Q. Wang, J.-J. Li, S.-F. Yuan, G.-J. Liang and Q.-M, *J. Am. Chem. Soc,* 2021., **143**, 17059-17067.

10. Z.-J. Guan, F. Hu, J.-J. Li, Z.-R. Wen, Y.-M. Lin and Q.-M. Wang, *J. Am. Chem. Soc.,* 2020, **142**, 2995-3001.

11. F. Hu, Z.-J. Guan, G. Yang, J.-Q. Wang, J.-J. Li, S.-F. Yuan, G.-J. Liang and Q.-M*, J. Am. Chem. Soc.*, 2021, **143**, 17059-17067.

12. S. K. Kailasa, T. P. Nguyen, S. H. Baek, R. Rafique and T. J. Park, *Talanta.*, 2019, **205**, 120087.

13. X. Yue, Q. Pan, J. Zhou, H. Ren, C. Peng, Z. Wang and Y. Zhang, *Food. Chem.*, 2022, **385**, 132670.

14. P. Huang, Q. Jiang, P. Yu, L. Yang and L. Mao, *ACS Appl. Mater. Interfaces.*, 2013, **5**, 5239−5246.

15. X Ma, Q Guo, Y Xie, H Ma, *Chem. Phys. Lett.*, 2016, **652**, 148−151.

16. B. Nieto-Ortega and T. Bürgi, *Acc. Chem. Res.*, 2018, **51**, 2811−2819.

17. X. Le Guével, B. Hötzer, G. Jung, K. Hollemeyer, V. Trouillet and M. Schneider, *J. Phys. Chem. C.*, 2011, **115**, 10955–10963.